A Community Seismic Network for the Early Detection of Seismic Activity Close to Active Volcanoes in Western El Salvador

Thomas H. W. Goebel*[1], Navin Thapa[1], Sadia Marium Rinty[1], Susana Delgado Andino[2], Adonay Martinez-Coto[2], Jaqueline Rivera[3], and Benancio Henriquez-Miranda[2]

Abstract

Seismic monitoring can provide key constraints on volcanic processes, magma migration, and preparatory processes before volcanic eruptions. Nevertheless, the high cost of broadband networks limits the number of volcanoes that are actively monitored. Here, we test the capability of a network of raspberry shake (RS) seismographs to monitor volcanoes in El Salvador and characterize associated seismicity sequences in real time. We deployed seven three-component, short-period RS velocity seismometers around Santa Ana volcano, which has a long history of phreatomagmatic eruptions as recently as 2007. The new network primarily supports training, research, and outreach activities but also has the potential to provide early alerts before volcanic unrest. The seismometers were installed at schools, a university campus, and hotels within 20 km of Santa Ana volcano. We recorded an accelerating seismicity sequence within ~15 km distance from the volcano between 28 December 2023 and 1 February 2024. Both magnitudes and seismicity rates increased systematically, culminating in two events above M_L 4 on 28 January 2024 without causing detectable changes in temperature or gas emissions at the summit of Santa Ana. Detailed space–time clustering analyses reveal dominant mainshock–aftershock triggering at local to regional distances, similar to tectonic earthquake sequences. The new RS network around Santa Ana volcano demonstrates the ability of low-cost seismometers to improve seismic event detection, location, and classification. The observations suggest that dense volcano monitoring networks facilitate an early detection of unfolding seismicity sequences and improve tectonic versus volcanic event classifications—a key component of reliable eruption alerts.

Cite this article as Goebel, T. H. W., N. Thapa, S. Marium Rinty, S. Delgado Andino, A. Martinez-Coto, J. Rivera, and B. Henriquez-Miranda (2025). A Community Seismic Network for the Early Detection of Seismic Activity Close to Active Volcanoes in Western El Salvador, *Seismol. Res. Lett.* **XX**, 1–12, doi: 10.1785/0220240343.

Supplemental Material

Introduction

Tectonic setting and volcanic activity

El Salvador is characterized by high seismic and volcanic hazards due to its location close to the Central American trench that extends from Mexico to Costa Rica (Harlow *et al.*, 1993). Volcanotectonic processes in the region are governed by the subduction of the Cocos plate underneath the Caribbean plate (Fig. 1). Rapid convergence rates of about 65–75 mm/yr generate high levels of seismicity and frequent felt events (Legrand *et al.*, 2020). The largest magnitude events are associated with the subduction zone with deepening seismicity to the northeast (Fig. 1; Ye *et al.*, 2013).

Our study area at the western edge of El Salvador spans from Lago Coatepeque in the east to the Cordillera de Apaneca and the city of Ahuachapan to the west and includes the Los Volcanes National Park (Fig. 1, Fig. S1, available in the supplemental material to this article). This park is a protected natural area with several active volcanoes, lagunas, and calderas. The topographically most striking features are the active Santa Ana and Izalco volcanoes, and the large caldera to the east, which includes Lago Coatepeque.

The Coatepeque caldera truncates the eastern side of the ancestral Santa Ana volcano. The 7 × 10 km wide caldera, now largely filled by a scenic lake, was formed during two major late-Pleistocene rhyodacitic pyroclastic-flow-producing eruptions (Siebert *et al.*, 2004). Volcanic activity moved to the

1. Center for Earthquake Research and Information, University of Memphis, Memphis, Tennessee, U.S.A., https://orcid.org/0000-0002-3154-425X (NT); 2. Multidisciplinary Faculty of the West, University of El Salvador, Santa Ana, El Salvador, https://orcid.org/0000-0002-9881-0217 (SDA); https://orcid.org/0009-0004-1970-0602 (AM-C); https://orcid.org/0009-0006-1065-3429 (BH-M); 3. Ministry of Environment and Natural Resources, San Salvador, El Salvador, https://orcid.org/0000-0003-2964-9471 (JR)

*Corresponding author: thgoebel@memphis.edu

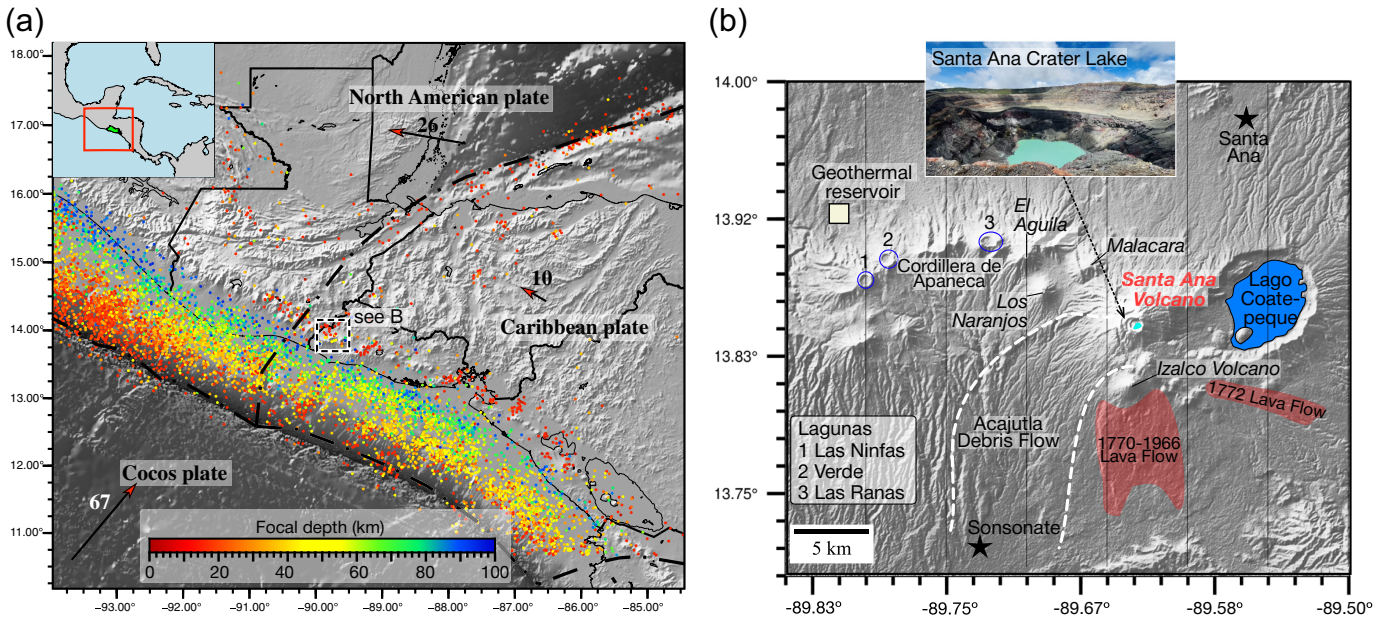

Figure 1. (a) Overview of seismicity and tectonic setting. Inset shows central America with El Salvador highlighted in green. Seismic activity is dominated by subduction zone events to the west (deepening toward the northeast) and shallow onshore seismicity. Relative plate motion of Cocos, Caribbean, and North American plates are highlighted by black arrows, and earthquakes are colored by depth (see color bar). Study area in western El Salvador is highlighted by blackdashed rectangle. Plate motion vectors are from Legrand *et al.* (2020). (b) Topography in the study area, which includes the Cordillera de Apaneca, Santa Ana and Izalco volcanoes, and Lago Coatepeque. Several additional prominent peaks that demonstrate widespread volcanic activity are labeled. Lagunas are highlighted by blue ellipses (see legend). Approximate extent of Acajutla debris flow and Izalco-Santa Ana lava flows are marked by white lines and red-shaded regions (Carr and Pontier, 1981; Siebert *et al.*, 2004). The Ahuachapan geothermal reservoir is highlighted by a white square. Inset shows summit photo of Santa Ana crater lake (taken September 2023). The color version of this figure is available only in the electronic edition.

southwest from the initial rhyolitic plinian eruptions of Coatepeque to the present activity at Santa Ana and Izalco. Magma sources for Coatepeque, Santa Ana, and Izalco exhibit notably different chemistry, in spite of their close proximity, resulting in markedly different types of eruptions (Rose and Stoiber, 1969; Scolamacchia *et al.*, 2010). Nearly contemporaneous eruptions of Santa Ana and Izalco over geological times highlight either efficient magma fractionation during ascent or distinct magma sources, with compositions ranging from basaltic to andesitic (Carr and Pontier, 1981). Izalco volcano, located ~4 km south and seaward of Santa Ana volcano, has produced predominately effusive eruptions since 1770, which ended in October 1966 (Rose and Stoiber, 1969; Carr and Pontier, 1981). At the time, the frequent eruptions with high lava discharge were widely visible by passing ships inspiring the name "Lighthouse of the Pacific" (Rose and Stoiber, 1969).

The Santa Ana volcanic complex displays the largest and highest stratovolcano in El Salvador (Pullinger, 1998). The broad flanks of the 2381-m-high basaltic-to-andesitic volcano extend north to the city of Santa Ana and south to Sonsonate, which are home to more than a million inhabitants combined (Fig. 1). In the late Pleistocene, the volcano collapsed and triggered a debris flow that traveled ~50 km south into the Pacific Ocean, with an estimated volume of 16 ± 5 km^3 (see label Acajutla debris flow in Fig. 1b; Siebert *et al.*, 2004). Eruptions of Santa Ana volcano are predominantly phreatic and phreatomagmatic and started in the late Pleistocene (0.22 Ma). The latest eruptions occurred in January 1904 (Volcanic Explosivity Index, VEI 2–3), 1 October 2005 (VEI 3), and 24 April 2007 (VEI 1; Laiolo *et al.*, 2017).

The 2005 eruption was the most notable event in recent history, producing a more than 10km high plume of gas and ash from the central crater (Scolamacchia *et al.*, 2010). Ash fallout traveled as far as 12 km and ballistic blocks and hot lahars reached a distance of up to 5 km (Hernández *et al.*, 2007; Scolamacchia *et al.*, 2010). The 2005 eruption was preceded by several weeks of precursory temperature increase, gas emissions, and a notable uptick in volcanotectonic and long-period (LP) seismic activity close to the summit (Hernández *et al.*, 2007; Olmos *et al.*, 2007; Laiolo *et al.*, 2017).

Previous seismic activity

Seismicity in the area is dominated by large offshore subduction zone events and shallower, onshore strike-slip earthquakes. The largest earthquakes in the broader area may reach $M_w \sim 7.9$ (Harlow *et al.*, 1993; Ye *et al.*, 2013) and are generated along the Cocos-Caribbean plate interface. Seismic and geologic observations suggest a large strike-slip

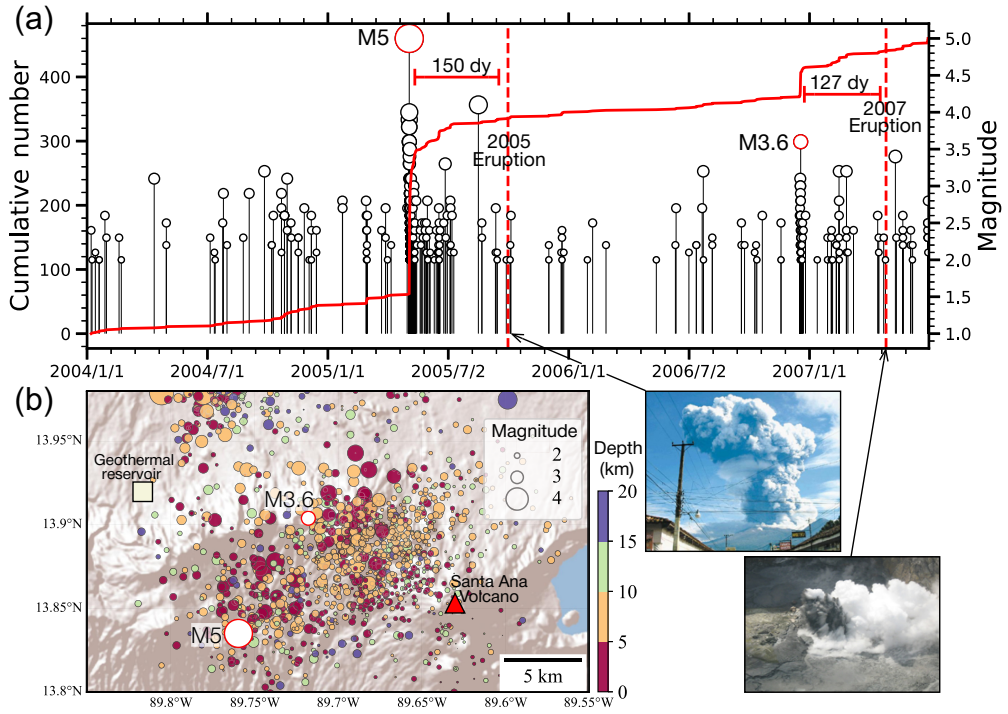

Figure 2. Earthquake magnitudes, cumulative number, and locations (Ministerio de Medioambiente y Recursos Naturales [MARN] catalog, see Section: "Previous seismic activity") before the 2005 and 2007 phreatomagmatic eruptions of Santa Ana volcano. (a) Time series of event magnitudes (black and red circles) and cumulative event number (red curve). Both eruptions were preceded by significant seismic activity 130–150 days prior. Note that no classification into volcanotectonic (VT) and long-period (LP) events was attempted by MARN, and the catalog may include both types of events. (b) Map of seismic activity shown in panel (a). Events are colored by depth, scaled by magnitude, and the largest events prior to the 2005 and 2007 eruptions are highlighted by red circles. Note that these events may have occurred far from the summit albeit location uncertainty is large 16. The two eruption photos at the lower right were taken on 1 October 2005 and 25 April 2007. The color version of this figure is available only in the electronic edition.

fault zone, the El Salvador fault zone, in the central part of the country (Martínez-Díaz *et al.*, 2004; Canora *et al.*, 2014). Shallower onshore faults have been responsible for the most destructive earthquakes in recent history, producing 22 moderate-to-large magnitude earthquakes above M 5 since 1700 with average recurrence of ~30 yr (Harlow *et al.*, 1993).

El Salvador was affected by two destructive earthquake sequences close to the capital city of San Salvador in 1986 and 2001. The M_w 5.7 San Salvador earthquake on 10 October 1986 ruptured a left-lateral strike-slip fault underneath the city, resulting in ~1500 deaths, ~10,000 injuries, and ~100,000 people left homeless (Harlow *et al.*, 1993). Strong ground motion lasted for only 3–5 s in most regions but basin effects may have contributed to significant destruction around the historic center of San Salvador (Anderson, 1987).

The second major earthquake ruptured a large portion of the right-lateral El Salvador strike-slip fault system about 30 km east of the capitol city on 13 February 2001 (Bommer *et al.*, 2002). This M_w 6.6 onshore event was preceded and potentially triggered by an M_w 7.7 event about 110 km south-southeast of San Salvador on 13 January 2001 (Martínez-Díaz *et al.*, 2004). The two events in January and February caused ~1000 deaths, ~7600 injuries, and destroyed ~84,000 houses, mainly due to the earlier, larger-magnitude earthquake (Bommer *et al.*, 2002; Parsons, 2002). The offshore event occurred on a normal fault within the subducting Cocos plate and caused particularly destructive landslides in addition to direct shaking-induced damage (Parsons, 2002).

Seismic triggering may have been responsible for both the 1986 and 2001 events. The underlying triggering mechanisms include static stress transfer from large offshore earthquakes to onshore faults (Martínez-Díaz *et al.*, 2004). Static or dynamic triggering is also thought to be responsible for several volcanic eruptions based on observed space–time correlations between earthquakes and subsequent volcanic eruptions. For instance, the San Salvador eruption close to the capital in 1917 was preceded by two destructive earthquakes (Legrand *et al.*, 2020), and the San Miguel eruption to the far east of El Salvador in 2013 was preceded by an anomalous sequence of three $M_w \geq 7.3$ events in 2012 (Ye *et al.*, 2013; Granieri *et al.*, 2015; Bonforte *et al.*, 2016; González *et al.*, 2021).

El Salvador produces about a quarter of its electricity from two large geothermal reservoirs, and operations at the Berlín geothermal field have led to felt, induced events up to M_w 3.7 (Herrera *et al.*, 2010; Kwiatek *et al.*, 2014). In contrast, the Ahuachapan geothermal field (white box in Fig. 1b), which is close to the here studied volcanoes, has no reported induced events to date.

High-resolution seismic monitoring is essential to better characterize the coupling between seismic and volcanic processes in El Salvador. For instance, the Apaneca-Juayua region just 10–20 km west of Santa Ana volcano produced two notable seismicity clusters 150 and 130 days before the 2005 and 2007 eruptions (Fig. 2). The respective seismicity catalog was created by the Ministerio de Medioambiente y Recursos Naturales (MARN) and is referred to as MARN catalog in

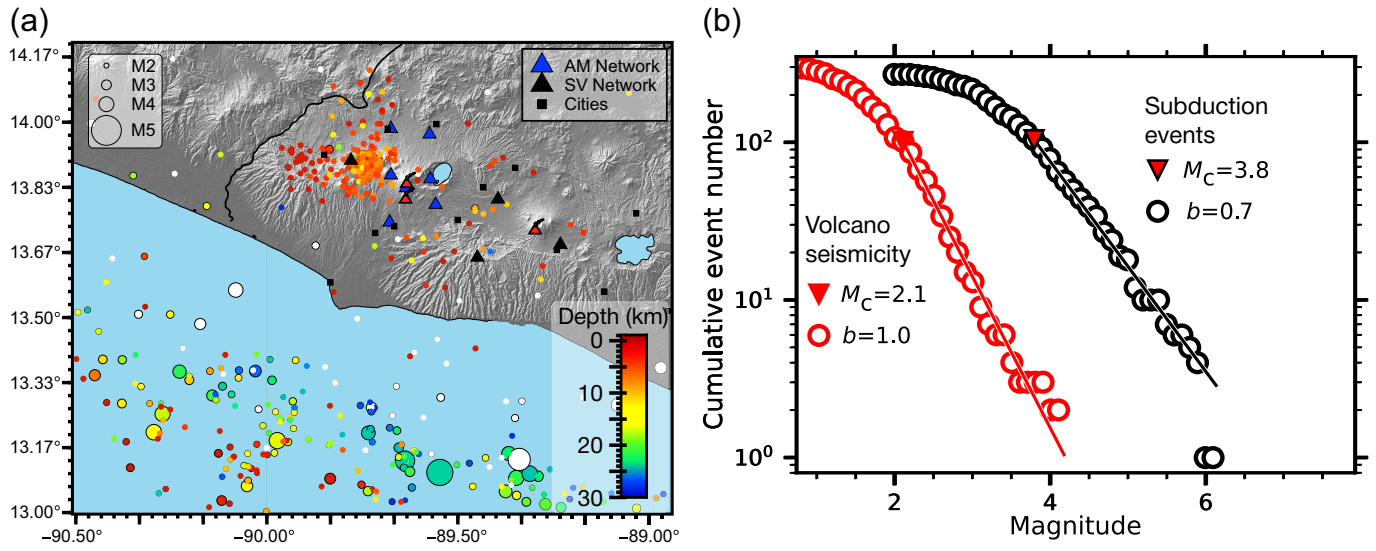

Figure 3. Overview of seismic network, event locations, and magnitudes between 25 November 2023 and 1 May 2024. (a) The seismicity map shows the two primary sources of seismic activity: (1) deeper offshore subduction zone events (colored markers with black circles) and (2) shallower onshore seismicity across the Cordillera de Apaneca. Newly deployed stations (AM network) are shown by blue triangles and SNET stations (network ID = SV) by black triangles. Station codes are in Figure S1. (b) Frequency–magnitude distributions of seismicity near the volcanic (red) and subduction (black) zones. Note the difference in magnitude of completeness and *b*-value. The color version of this figure is available only in the electronic edition.

the following. Unfortunately, most earthquake locations were based on fewer than five phase picks, which hamper in-depth analyses as described subsequently, and only a single station (SBLS) was operational at Santa Ana volcano at the time of the 2005 eruption (Olmos *et al.*, 2007; Laiolo *et al.*, 2017). The new stations deployed in this study significantly improved this situation.

Data and Method

Seismic network deployment and operation

Motivated by the previous volcanic and seismic activity across the study area, we densified the regional broadband network around Santa Ana volcano (see new raspberry shake [RS] network, FDSN code = AM vs. previous stations from the El Salvador network, FDSN code = SV, of the Servicio Nacional de Estudios Territoriales de El Salvador in Fig. 3). Before the new deployment, only one station (NUBE) with direct data access through the Incorporated Research Institutions for Seismology was located within 30 km of Santa Ana volcano. The new network deployment had three primary goals.

1. **Education and outreach:** we worked with partners from the University of El Salvador, MARN, schools, residents, and businesses to improve hazard awareness and preparedness. For this purpose, we decided to install inexpensive RS seismometers mainly at schools and educational centers. Station deployments were paired with educational and informational activities including several teachers workshops at the University of El Salvador.
2. **Training:** we supported the natural hazards curriculum at the physics department at the University of El Salvador through several seismology short courses and trained local students in real time seismic data processing. The university partners identified the most suitable sites and participated in all station deployments. A group of five students from the university received training in how to operate the seismometers and how to generate real-time seismicity catalogs in SeisComP (SeisComP, 2008).
3. **Research:** the local, dense network comprised seven RS3D seismographs, which, together with the SV broadband stations, provide new insights into tectonic, magmatic, and volcanic processes across the study area. Moreover, the new network has proven capable to rapidly detect unfolding seismic sequences as detailed in the following sections.

In addition to the described RS3D stations, our combined network includes four broadband stations that are operated by MARN and one Güralp CMG6TD at the University of El Salvador, Multidisciplinary Faculty of the West in Santa Ana (Fig. S1). The new stations were deployed indoors at ground level. RS3D stations determine 3D ground motion from 4.5 Hz geophones electronically extended down to 2 s and sampled at 100 Hz. Corresponding clip level are 24 mm/s peak-to-peak from 0.1 to 10 Hz.

This study describes data acquired between 1 December 2023 and 1 May 2024. Seedlink data streams were received by two SeisComP servers in real time—one at the University of El Salvador, Multidisciplinary Faculty of the West, and the other at the Center for Earthquake Research and Information, University of Memphis. The duplicate data

servers prevent data loss in case of power or internet outages. Data recovery rates for the RS stations range between 75% and 85% due to power and internet outages at the deployment sites.

The RS instruments can be controlled remotely through a zero-trust, peer-to-peer network using the zerotier service. Data from the RS stations can also be viewed by all community partners through a web interface (see Data and Resources), which is particularly useful for educational activities. RS instruments have been used in several applications, such as network densification and rockfall detection (Manconi *et al.*, 2018; Walter *et al.*, 2019; Calais *et al.*, 2020), but this work is potentially the first attempt to build a real-time volcano monitoring network with RSs.

Exemplary seismic events and noise characteristics

The current results illustrate the usefulness of low-cost station densifications, in particular for the improvement of azimuthal coverage, phase picks, and location accuracy. Without the short-period instruments most of the small-magnitude local events would be difficult to detect and locate (Figs. S2, S3). Such events are well-recorded between ~2 s and ~40 Hz, in spite of the relatively higher self-noise of the instruments (Anthony *et al.*, 2019) and transient, high-frequency anthropogenic noise (Figs. S4, S5).

We identified three primary event types (Fig. S5; McNutt, 2005): (1) local, high-frequency volcanotectonic (VT) events within about 20 km of the volcano, (2) distant earthquakes with longer duration and *S-P* times of more than ~10 s, and (3) low-amplitude, LP events that likely originate from large depths. Although the proximal and distal earthquakes show two distinct, impulsive body-wave arrivals, the LP events show no distinguishable seismic phases.

LP events were detected manually based on time and frequency characteristics. Commonly observed event attributes were long duration (i.e., >20 s), small amplitude, and lack of seismic energy above 5 Hz (Fig. S5). The LP events compose only a small fraction of the total events (<1%). Preliminary analysis suggests that the LP events are not related to shallow magmatic processes but rather occur deeper and about 50 km seaward of Santa Ana volcano. In the following, we focus on proximal, high-frequency earthquake sources, which constitute the vast majority of all detections.

Seismicity catalog creation

Real-time data processing is done in SeisComP (SeisComP, 2008). We use a STA/LTA detector and AIC picker to determine P-onsets and *locsat* for automatic locations. Each event is manually revised by student analysts, including P-pick refinement, adding new S-picks, and determining local magnitudes. Events were kept if travel time residuals were less than 0.5 sec and the event had six or more phase picks across at least four stations.

Local magnitudes were calculated from peak body-wave amplitudes (mainly *S* waves), which were corrected for source–receiver distances using Bakun and Joyner (1984) and then averaged over stations within a plausible range. We determined *b*-value and the magnitude of completeness by minimizing the misfit between observed and modeled earthquake magnitude distributions, using a maximum-likelihood approach and a Kolmogorov–Smirnov (KS) misfit measure (Goebel *et al.*, 2017; Fig. S6). To avoid selecting a magnitude of completeness in the tail of the distribution, we use only values of minimum KS-distances, which also have a standard error of *b*-value estimates below 0.25 (Shi and Bolt, 1982; Goebel *et al.*, 2017).

A first assessment of the local magnitudes shows Gutenberg–Richter behavior for local events with magnitudes between two and four. Nevertheless, we also observe overestimated magnitudes compared to the European-Mediterranean Seismological Centre catalogs, especially for subduction zone events. This comparison highlights the need for refined local and moment magnitude estimates in the future.

Results

High-resolution seismic event locations can provide important insight into magmatic processes. The 2005 Santa Ana eruption was preceded by several weeks of precursory seismic activity (Laiolo *et al.*, 2017) and an early seismicity cluster 150 days before the eruption may have marked the onset of intensifying magmatic processes (Fig. 2). In the following, we elucidate the creation of an improved seismicity catalog for the study area. We first describe observations in the initial SeisComP catalog and then report additional catalog refinements, including improved velocity models, absolute locations, and double-difference relocations.

Our initial catalog contains 798 events and clearly delineates near-volcano seismic sources at depths between ~1 and 10 km from deeper subduction zone events (Fig. 3). The two event populations have markedly different magnitude distributions, with higher completeness magnitude and lower *b*-value for the distant subduction zone events (i.e., $M_c = 3.8$ compared to $M_c = 2.1$). Interestingly, we also find a day–night dependence of completeness magnitude for the near-volcano events so that M_c drops from 2.1 to 1.4 during low-noise night hours (Fig. S6). The notable shift in completeness can be explained by the relatively higher noise at schools during the day compared to quieter nights.

We use the initial catalog as the starting point for velocity model and location refinements for events within 20 km from the summit of Santa Ana volcano. The initial IASP91 velocity model is constant in the upper 20 km. We use VELEST for an improved 1D velocity model (Kissling *et al.*, 1994) that includes three layers from 0 to 5, 5 to 10, and 10 to 20 km (Fig. 4). The resulting seismic velocities are reduced by ~10% in the upper 5 km. We confirm the overall robustness of the simple velocity

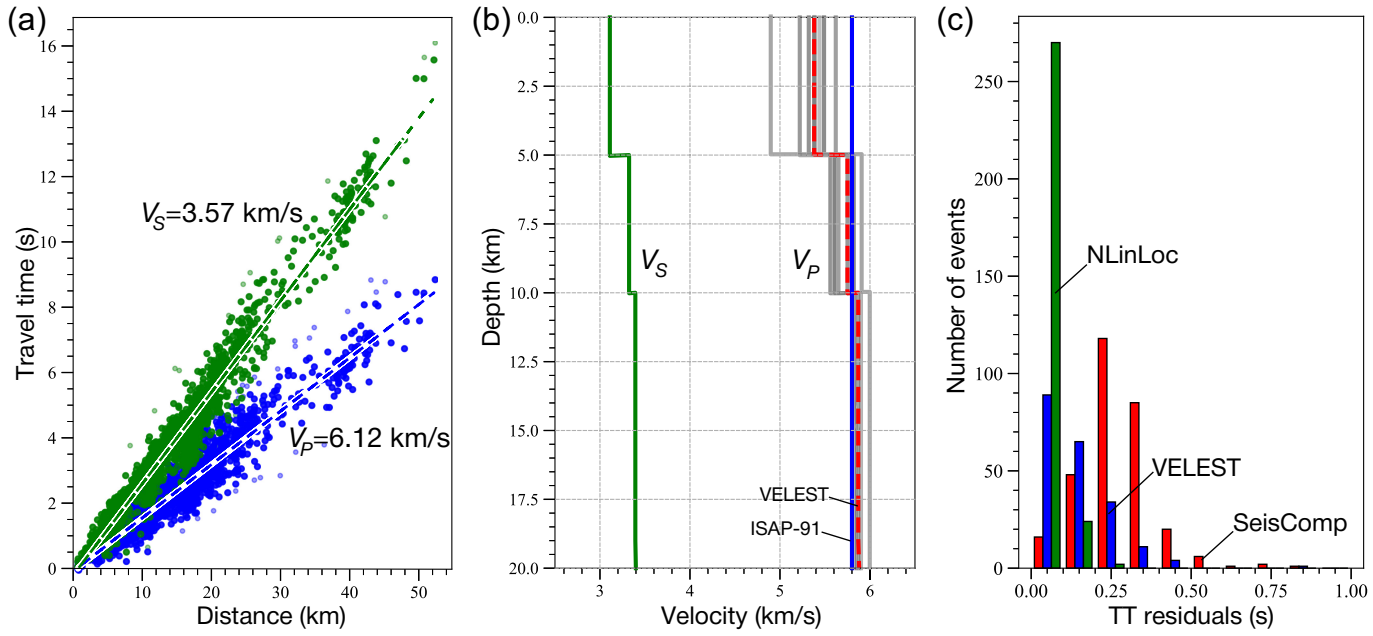

Figure 4. (a) Travel-time plot and average seismic velocities from the initial catalog. (b) Refined velocity model for the upper 20 km of the study area. Starting *P*-wave velocity (V_P) model is shown in blue and new model in red with gray lines showing results from jackknife resampling across the network stations. Note that V_S was determined from constant $V_P/V_S = 1.71$. (c) Improvement in travel-time residuals (root mean square [rms] over all stations with picks) between initial SeisComP catalog (red), VELEST (blue), and NLLoc (green) locations. The color version of this figure is available only in the electronic edition.

model through jackknife resampling across stations, which shows the effect of individual station pick errors (Fig. 4b). Next, we use the velocity model and station terms from VELEST to relocate the earthquakes with NLLoc (Lomax *et al.*, 2009). These different steps lead to a notable reduction in overall travel-time residuals compared to the original catalog (see Fig. 4c)

We relocated the seismicity within 20 km from Santa Ana volcano between 31 November 2023 and 1 May 2024 with GrowClust using waveform cross correlations (CCs) and differential travel times of *P* and *S* waves at each station (Fig. 5) (Trugman and Shearer, 2017). CCs were computed on band-passed waveforms from 2 to 8 Hz, starting 0.2 s before and 0.3 s after *P* and *S* picks. We use a minimum CC coefficient of 0.5 for each event (see Fig. S7 for results with different CC thresholds). The maximum root mean square (rms) travel-time residual is limited to 0.3 s. This results in the relocation of 225 out of the original 297 events, with relative horizontal and vertical errors of 0.4 km (Fig. S8).

The double-difference relocated catalog shows two distinct seismicity clusters, which are not easily identifiable in the original catalog (Fig. 5). The first cluster is located at shallower depth between 5 and 8 km in direct proximity to station NUBE. The second cluster is deeper between 8 and 12 km depth, located ~2 km farther east toward Santa Ana volcano. These two clusters mark different stages of the accelerating seismic activity and are potentially connected to the activation of different fault structures.

Seismicity characteristics and rate increase between November 2023 and February 2024

The new network deployment was associated with a notable increase in seismic activity between 28 December 2023 and 1 February 2024. This activity included at least three events that were felt by the nearby population and was of significant concern for scientists from MARN, the University of El Salvador and the University of Memphis, not least due to the extended seismic activity in the same area before the 2005 eruption of Santa Ana volcano.

The seismic network started operations in mid-December, although limited earlier detection was possible with a subset of the final network stations starting on 25 November 2023. A first productive seismicity cluster was recorded just after Christmas in 2023 with a maximum magnitude of M_L 2 and a minimum magnitude of M_L 0.5 (Fig. 6). The subsequent activity continued to exhibit strong temporal clustering, and rates and magnitudes increased systematically, culminating in a pair of M_L 4 events in the eastern cluster on 28 January. These events were felt by the nearby population, primarily in the town of Juayua (Fig. 6).

The activity prior to 28 January was concentrated within the western cluster in Figure 5b. Activity then migrated deeper (Fig. S9) and to the east toward Santa Ana volcano. The gradually unfolding seismicity sequence was closely monitored and discussed with the colleagues from the University of El Salvador and MARN, and motivated an inspection of volcanic activity at the summit. However, no changes in lake level, temperature, or gas emissions were observed. The subsequent

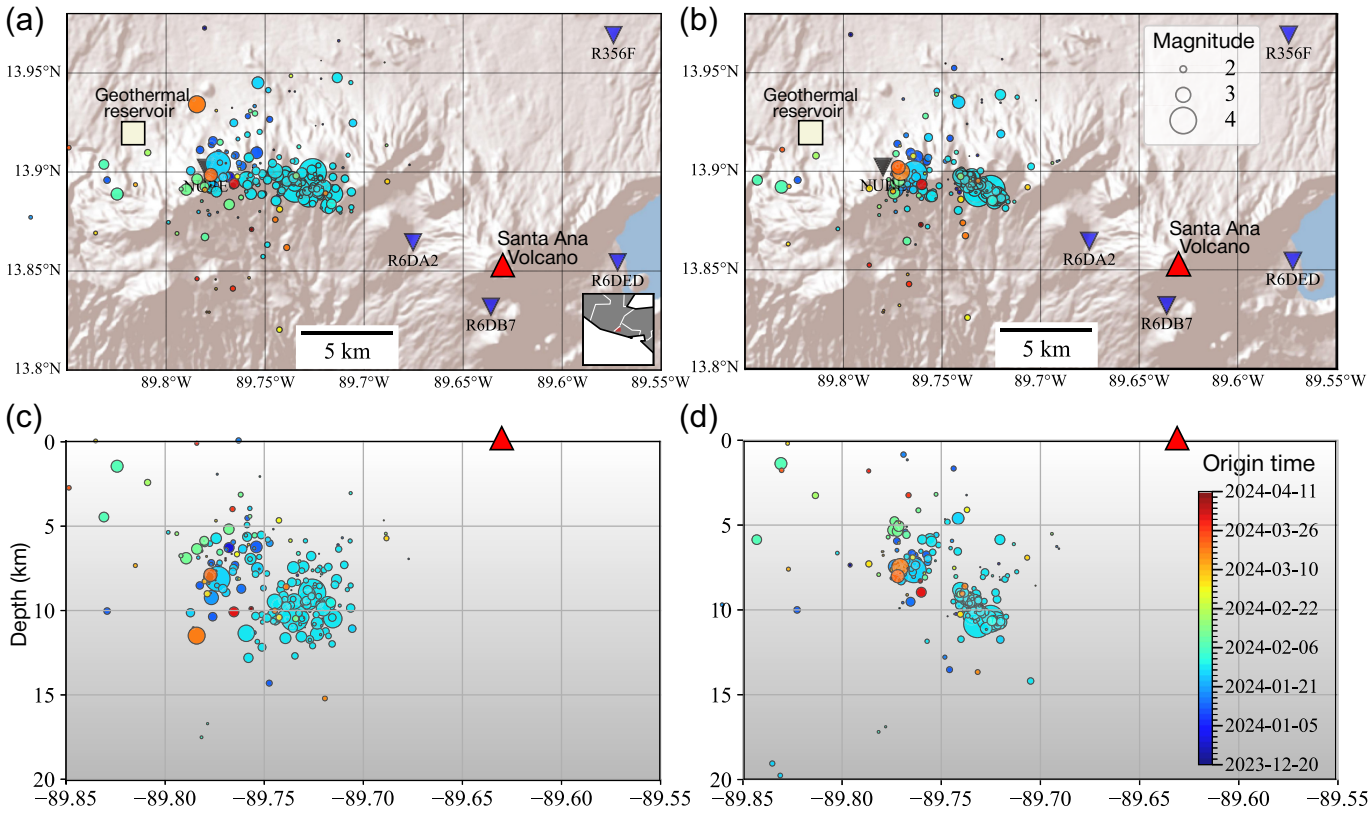

Figure 5. Seismic event locations before and after waveform cross correlation and double-difference relocation. (a,c) Map and depth cross section of event locations in the NLLoc catalog. Inset in (a) shows study area in central America. (b,d) Map and depth cross section of event locations in the relocated catalog. Note the two distinct clusters at 5–8 and 8–12 km depths, respectively. The color version of this figure is available only in the electronic edition.

seismic activity was characterized by lower rates and magnitudes ($M_{max} = 3.6$) until the end of the analysis period on 1 May 2024.

We conducted a detailed analysis of the unfolding seismic activity between 28 December 2023 and 1 February 2024 and quantified the degree of space–time clustering, which may be indicative of tectonic or volcanic processes. The seismicity clusters migrated from west to east toward Santa Ana volcano at about 0.3 km/day until the occurrence of the largest events on 28 January 2024, and subsequently, reversed its direction (Fig. 7a). We searched for potential migratory signals within individual clusters and observed very rapidly unfolding activity within <1 day across distances of 0–7 km from the largest event (Fig. 7b). The lack of detectable event migration within clusters may suggest that event interactions are dominated by elastic stress transfer, which is investigated in the following.

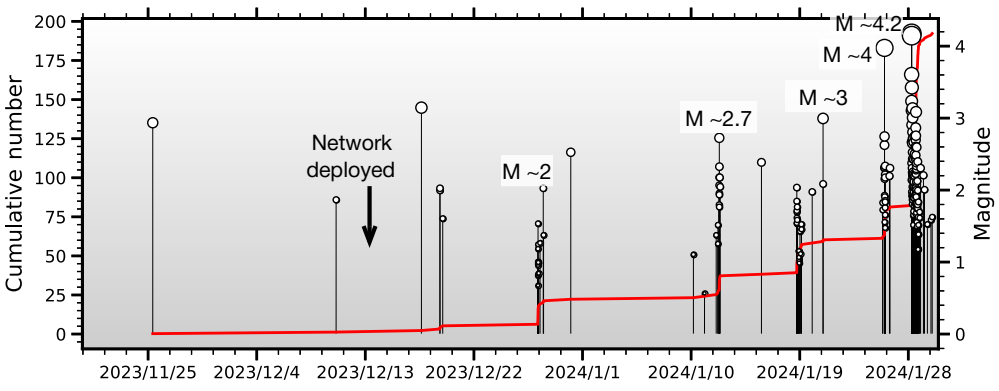

Figure 6. Time series of magnitudes (black circles) and cumulative event number (red curve) of unfolding seismic sequences between 28 December 2023 and 1 February 2024. Network was operational after 13 December 2023. Rate and magnitudes of seismic events increased until the end of January 2024, when two events with $M_L \sim 4.2$ were recorded. The color version of this figure is available only in the electronic edition.

Space–time clustering characteristics

To further understand potential driving mechanisms of

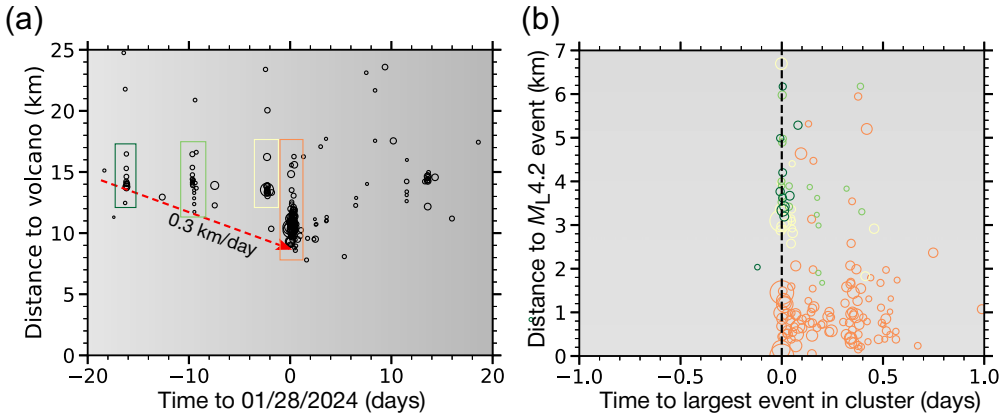

Figure 7. (a) Seismicity (black circles) migrated to the east toward Santa Ana volcano prior to the $M_L \sim 4.2$ event on 28 January 2024, followed by migration in the opposite direction. (b) Timing of events within individual clusters (colors correspond to rectangles in panel a) relative to the largest event in each cluster, and distance to the $M_L \sim 4.2$ event on 28 January 2024. Note that no migration is observed within the individual clusters. The color version of this figure is available only in the electronic edition.

the earthquake sequences, we performed a nearest-neighbor-clustering analysis (Zaliapin and Ben-Zion, 2013a). This analysis is particularly useful to distinguish tectonic, human-induced, and natural swarm activity (Zaliapin and Ben-Zion, 2013b, 2016). For each seismic event j in the catalog, we determined its unique parent i with the smallest nearest-neighbor distance η in a space–time–magnitude domain:

$$\eta_{ij} = t_{ij}(r_{ij})^{d_f} 10^{-bm_i}, \quad t_{ij} > 0, \tag{1}$$

in which t and r are interevent time and distance, respectively; d_f is the fractal dimension; b is the exponent of the magnitude distribution; and m is the magnitude. The fractal dimension is computed by fitting the correlation integral over a distance range for which the distribution appears linear after log transformation (Goebel *et al.*, 2017), resulting in $d_f = 1.0 - 1.4$, which indicates a very high degree of spatial clustering.

The histogram of nearest-neighbor distances is characterized by two distinct modes, at $\log_{10}\eta = -7.9$ and $\log_{10}\eta = -4.5$ (Fig. S10). These two modes are typical for triggered and independent background events. We test the separation of independent and triggered events by removing inherent space–time clustering through reshuffling in the space and time domain and confirm that a value of $\log_{10}\eta_0 = -6$ provides a clear separation between clustered and independent background events. The corresponding value is determined from the 99th percentile of η in randomized catalogs (Goebel *et al.*, 2019). We further test the sensitivity of the results by varying M_c between 1.4 and 2.1 and d_f between 1.0 and 1.4 and find no significant difference in clustering characteristics, in agreement with previous sensitivity tests (Zaliapin and Ben-Zion, 2013a).

We further compare clustering characteristics of seismicity catalogs between southern California ($d_f = 1.4$, $b = 0.9$, see Data and Resources), the older MARN catalog ($d_f = 1.8$, $b = 0.9$) between 1 January 2004 and 1 July 2007 (see Fig. 2) and our new catalog ($d_f = 1.4$, $b = 1.0$) from 1 December 2023 to 1 May 2024. For this purpose, we separate the nearest-neighbor distance into rescaled interevent time T_{ij} and distance R_{ij} using

$$T_{ij} = t_{ij}10^{-0.5bm_i};$$
$$R_{ij} = (r_{ij})^{d_f}10^{-0.5bm_i};$$
$$\text{and } \eta_{ij} = T_{ij}R_{ij}. \tag{2}$$

The 2D probability density functions in the R-T domain commonly show two dominant modes for background and clustered events, similar to the η histograms, but now the modes are shifted in space and time (see Fig. 8a; Zaliapin and Ben-Zion, 2013a). Some catalogs exhibit a third mode at small R and large T due to repeating earthquakes or human-induced seismicity (Goebel and Shirzaei, 2021), the latter also showing a more dominant background mode (Zaliapin and Ben-Zion, 2016).

The relocated Santa Ana catalog exhibits a dominant clustered mode at small R-T, indicative for strong event interactions (compare Fig. 8a and Fig. 8c). The clustered mode has a centroid at $\log_{10} T = -6$ and $\log_{10} R = -2$, similar to observations in southern California. The Santa Ana catalog is composed of 69% clustered events versus 66% in the southern California catalog and ~75% in the MARN catalog. The MARN catalog between 2004 and 2008 exhibits a high degree of temporal clustering due to two moderate-magnitude earthquake sequences with many aftershocks in 2005 and 2006. Nearest neighbors are farther disbursed in R, likely due to higher location uncertainty.

We further investigate clustering characteristics by computing average leaf depth $<d>$ of event families and find dominant aftershock-burst characteristics (Fig. 9; Zaliapin and Ben-Zion, 2013b). The topology of clustered families can be used to distinguish fluid-driven swarms with high-average leaf depth (i.e., many trigger generations, see Fig. 9c) versus tectonic aftershock bursts with low-average leaf depth (i.e., few trigger generations, see Fig. 9d; Zaliapin and Ben-Zion, 2013b). The clustered families in our catalog exhibit average leaf depth below 4, which again is indicative for efficient direct triggering. The same topology is observed in epidemic-type aftershock sequence catalogs with dominant event–event interactions and direct triggering as the primary process that causes event clustering (Zaliapin and Ben-Zion, 2013b).

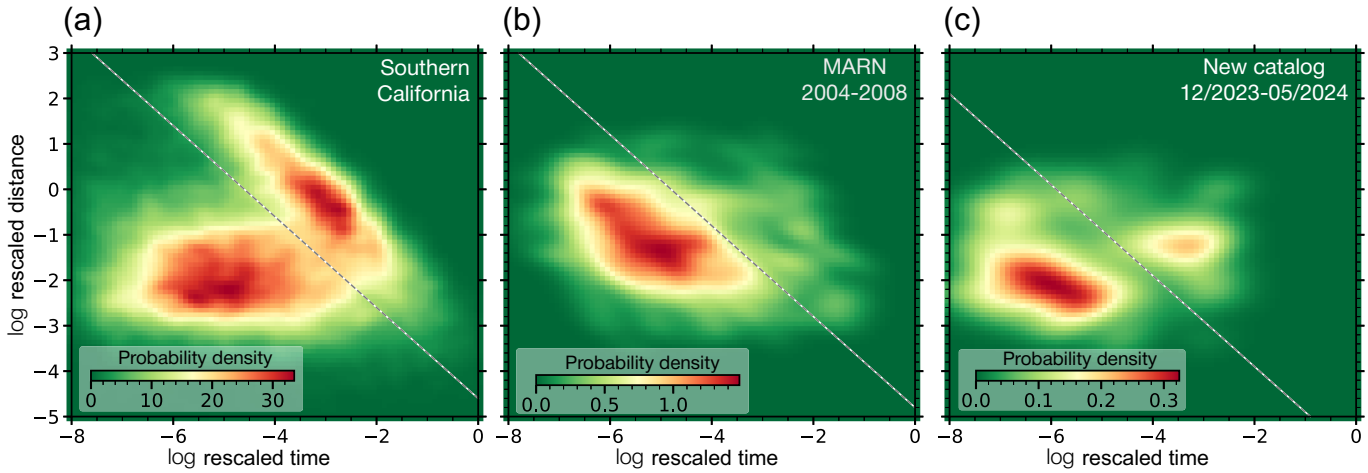

Figure 8. Space–time clustering of seismic events close to Santa Ana is dominated by triggered events, similar to active tectonic regions. (a) Nearest-neighbor distance and time rescaled by parent event magnitude for southern California are shown here. (b) The Santa Ana seismicity catalogs from MARN between 2004 and 2008. (c) The new catalog between 28 December 2023 and 1 May 2024. Colors correspond to event-pair density (see color bar). Southern California and the new Santa Ana catalog exhibit a bimodal distribution (see also Fig. S10) consisting of triggered and background mode whereas the previous MARN catalog showed a single mode. The color version of this figure is available only in the electronic edition.

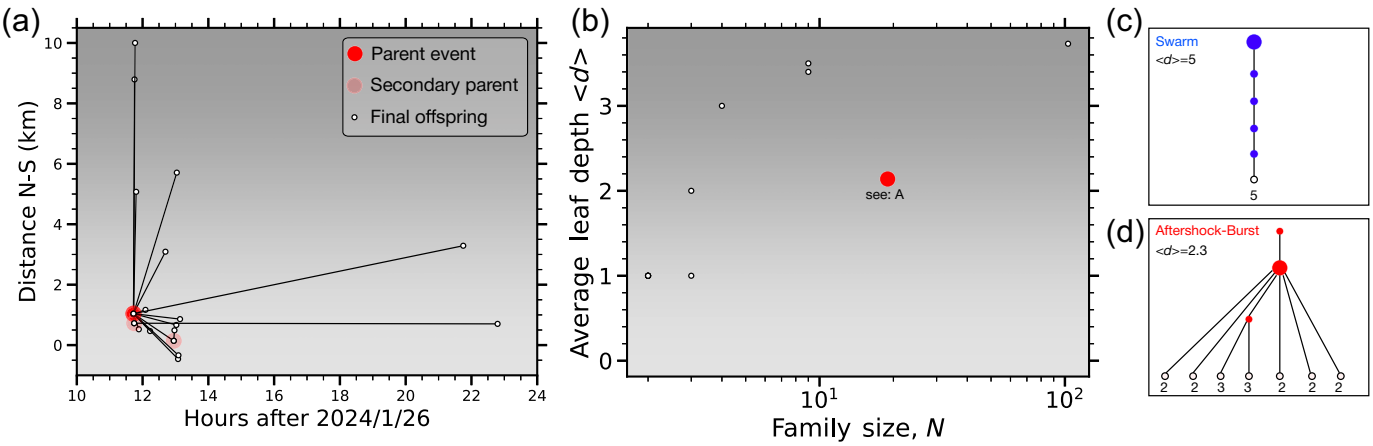

Figure 9. The new Santa Ana catalog is dominated by burstlike aftershock sequences. (a) Cluster topology of an exemplary earthquake sequence (see yellow box in Fig. 7a) with average leaf depth of 2.2 (see panel b) on 26 January 2024. (b) Average leaf depth and family size for all clustered events. (c,d) Schematic illustration of swarms versus aftershock bursts. Swarms are expected to have larger average leaf depths whereas aftershock bursts are characterized by one dominant parent that is directly linked to most offspring (aftershocks). The color version of this figure is available only in the electronic edition.

Based on the lack of earthquake migration within clusters, high degree of space–time clustering, and focal depths (Fig. S9), we conclude that the observed seismic activity close to Santa Ana volcano shows little evidence for hydrothermally and magmatically driven swarms. Rather, the statistical properties are characteristic for aftershock bursts for which subsequent events are caused by stress perturbations (e.g., static or dynamic) from the parent event.

The susceptibility of seismicity to triggering stresses is further supported by a significant rate increase within 36 hr after an M_w 6.1 event at a distance of ~150 km on 27 January 2024 (Fig. 10). Corresponding dynamic strains, estimated from peak shear-wave amplitudes across the Santa Ana stations, are between 6×10^{-7} and 3×10^{-6}, and dynamic stresses were between 19 and 90 kPa. The large rate jump could be indicative of dynamically triggered events on a critically stressed fault. Notably, regional scale interactions may not only be important for seismic event triggering but also volcanic eruptions (González *et al.*, 2021).

Discussion

The new dense RS network around Santa Ana volcano demonstrates the ability of low-cost seismometers to improve

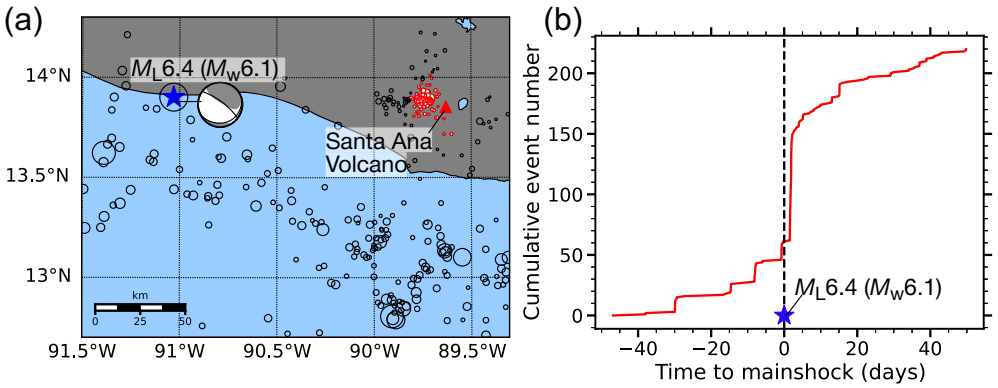

Figure 10. The largest event in the catalog (i.e., M_L 6.4 on UTC 27 January 2024 05:52:48.42) is associated with a significant increase in seismicity rate close to Santa Ana volcano. (a) Map of M_L 6.4 (M_w 6.1) event offshore Guatemala (blue star with focal mechanism from U.S. Geological Survey [USGS]) and Santa Ana seismicity (red circles). (b) Cumulative number of events within the study area ±50 days from the M_L 6.4 event. The color version of this figure is available only in the electronic edition.

seismic monitoring through local network densification. The new network has generated three major benefits.

1. The new network can be used as a key component in a volcanic eruption alert system. The observations suggest that the dense networks facilitated an early detection of an accelerating seismic sequence in 2023 and 2024 by reducing the magnitude of completeness in the study area. Completeness is strongly affected by anthropogenic noise at each site. Further improvements are likely possible by identifying quieter sites.
2. The real-time public data streams support the training of students at the University of El Salvador and are well suited to support education and outreach efforts at schools and other deployment sites. The RS system provides direct data viewing capabilities through a web interface. In addition to frequent school visits and direct communication with teachers, the project team has conducted two different education and outreach workshops at the University of El Salvador, Multidisciplinary Faculty of the West, with the goal to communicate scientific insight and improve hazard preparedness.
3. The seismicity catalogs have produced important scientific insights into event clustering characteristics and underlying mechanisms. The observed space–time clustering is indicative of direct triggering and efficient static or dynamic stress loading of critically stressed faults. The statistical properties of the here described event families are characteristic for aftershock bursts. Interestingly, the background mode is much less pronounced in the study area compared to, for example, southern California. These observations indicate the overall sensitivity to small triggering stresses, which is also supported by the increase in seismic activity after an M_w 6.1 event on 27 January 2024.

Large-scale interaction between intraslab normal-faulting events in the central American subduction zone and onshore strike-slip faults may have been responsible for notable seismic events in El Salvador in 1986 and 2001 (Martínez-Díaz *et al.*, 2004). The potentially triggered onshore activity may occur with lag times between one day, as observed here, or up to four weeks, as observed in 2001 (Parsons, 2002).

Large offshore events can also lead to triggered volcanic eruptions. For instance, in 2012, three large subduction earthquakes above M_w 7 occurred in central America within a period of 10 weeks, followed by more frequent eruptions within days to months (Ye *et al.*, 2013; González *et al.*, 2021). The eruption of San Miguel volcano in eastern El Salvador on 29 December 2013 after 46 yr of relative quiescence may be linked to long-range interactions between earthquakes and volcanoes (Granieri *et al.*, 2015; Bonforte *et al.*, 2016). Underlying mechanisms may include static and dynamic stress transfer processes. These observations highlight the importance of improved local and regional scale monitoring to detect triggering and potential premonitory signals before volcanic eruptions.

High-resolution local networks and detailed clustering analysis provide important tools to differentiate magmatic from tectonic processes. Differentiating such processes is especially important in Santa Ana and San Salvador where seismogenic faults are collocated with the central American volcanic arc (Harlow *et al.*, 1993; Legrand *et al.*, 2020). Seismicity clusters that are driven by hydrothermal fluids and high heat flow are thought to be similar to induced seismicity, exhibiting a high fraction of background events, strong spatial clustering, only modest temporal clustering and many generations of triggered events (i.e., high $<d>$; Goebel and Shirzaei, 2021; Zaliapin and Ben-Zion, 2013b, 2016). Conversely, our Santa Ana catalog is dominated by highly clustered, burstlike sequences and very few background events. Average leaf depths are small, contrary to swarm activity with higher leaf depth (Zaliapin and Ben-Zion, 2013b). We conclude that systematic differences in clustering characteristics can be an important component in identifying driving mechanisms of seismicity sequences.

Conclusion

El Salvador is one of the seismically most active countries in central America. We presented results from high-resolution

seismicity analyses using an RS network within ~20 km from Santa Ana volcano. The new network is fulfilling three primary goals: (1) to train local students and seismic analysts, (2) to provide education and outreach opportunities to local schools and to improve volcano and seismic hazard preparedness, and (3) to provide scientific insight and early alerts before volcanic eruptions.

The network recorded offshore events with a completeness magnitude of $M_c = 3.8$ and onshore seismicity around Santa Ana volcano with a completeness magnitude of $M_c = 1.4$ (nighttime)–2.1 (daytime). We detected an accelerating seismicity sequence with events up to M_L 4.2 that did not lead to an increase in volcanic activity between December 2023 and February 2025. Detailed space–time clustering analysis suggests a tectonic origin of the sequence.

We resolved a notable increase in seismicity rates in the study area after an M_w 6.1 subduction zone event at a distance of ~150 km. Previous observations suggest that large-magnitude offshore earthquakes can trigger seismic and volcanic activity across the Central American trench; however, improved long-term monitoring is needed to clearly resolve potential triggering effects. This study demonstrates the overall capabilities of low-cost seismic networks to rapidly detect unfolding seismicity sequences and to differentiate tectonic and magmatic processes. Local and regional seismic monitoring is essential for improved hazard assessment across the Central America volcanic arc.

Data and Resources

Raspberry shake (RS) station locations and seismic data can be viewed and accessed at https://stationview.raspberryshake.org/ (last accessed March 2025). The analysis of the seismic waveforms was primarily conducted with ObsPy (Beyreuther *et al.*, 2010; Krischer *et al.*, 2015). Seismicity catalogs are accessible at https://data.mendeley.com/datasets/b5tct3xpp7/1 (last accessed March 2025), "Santa Ana volcano seismicity," Mendeley Data, V1, doi: 10.17632/b5tct3xpp7.1. The relocated seismicity catalog for southern California between 1981 and 2018 can be accessed via https://scedc.caltech.edu/data/alt-2011-dd-hauksson-yang-shearer.html (last accessed March 2025). Clustering analysis codes are available at https://github.com/tgoebel/clustering-analysis (last accessed March 2025). The supplemental material includes an animation that shows the unfolding seismic activity and a PDF document with deployment photos, earthquake waveforms, and further details of seismicity statistics and relocation results.

Declaration of Competing Interests

The authors acknowledge that there are no conflicts of interest recorded.

Acknowledgments

The authors would like to thank Jeremy Pesicek and the associate editor for detailed reviews of an early version of this work. This research was supported by the National Science Foundation (NSF) Grant 2142489 to T. G.

References

Anderson, R. W. (1987). The San Salvador earthquake of October 10, 1986-review of building damage, *Earthq. Spectra* **3,** 497.

Anthony, R. E., A. T. Ringler, D. C. Wilson, and E. Wolin (2019). Do low-cost seismographs perform well enough for your network? An overview of laboratory tests and field observations of the OSOP raspberry shake 4D, *Seismol. Res. Lett.* **90,** 219–228.

Bakun, W. H., and W. B. Joyner (1984). The ml scale in central California, *Bull. Seismol. Soc. Am.* **74,** 1827–1843.

Beyreuther, M., R. Barsch, L. Krischer, T. Megies, Y. Behr, and J. Wassermann (2010). Obspy: A python toolbox for seismology, *Seismol. Res. Lett.* **81,** 530–533.

Bommer, J., M. Benito, M. Ciudad-Real, A. Lemoine, M. López-Menjívar, R. Madariaga, J. Mankelow, P. M. de Hasbun, W. Murphy, M. Nieto-Lovo, *et al.* (2002). The El Salvador earthquakes of January and February 2001: Context, characteristics and implications for seismic risk, *Soil Dynam. Earthq. Eng.* **22,** no. 5, 389–418.

Bonforte, A., D. A. Hernandez, E. Gutiérrez, L. Handal, C. Polío, S. Rapisarda, and P. Scarlato (2016). The unrest of the san Miguel volcano (El Salvador, Central America): installation of the monitoring network and observed volcano-tectonic ground deformation, *Nat. Hazards Earth Syst. Sci.* **16,** 1755–1769.

Calais, E., D. Boisson, S. Symithe, C. Prépetit, B. Pierre, S. Ulyse, L. Hurbon, A. Gilles, J. M. Théodat, T. Monfret, *et al.* (2020). A socio-seismology experiment in Haiti, *Front. Earth Sci.* **8,** doi: 10.3389/feart.2020.542654.

Canora, C., J. J. Martínez-Díaz, P. Villamor, A. Staller, K. Berryman, J. A. Álvarez Gómez, R. Capote, and M. Diaz (2014). Structural evolution of the El Salvador fault zone: An evolving fault system within a volcanic arc, *J. Iberian Geol.* **40,** 471–488.

Carr, M. J., and N. K. Pontier (1981). Evolution of a young parasitic cone towards a mature central vent Izalco and Santa Ana volcanoes in el Salvador, central America, *J. Volcanol. Geotherm. Res.* **11,** 277–292.

Goebel, T., Z. Rosson, E. Brodsky, and J. Walter (2019). Aftershock deficiency of induced earthquake sequences during rapid mitigation efforts in Oklahoma, *Earth Planet. Sci. Lett.* **522,** 135–143

Goebel, T. H., G. Kwiatek, T. W. Becker, E. E. Brodsky, and G. Dresen (2017). What allows seismic events to grow big? Insights from b-value and fault roughness analysis in laboratory stick-slip experiments, *Geology* **45,** 815–818.

Goebel, T. H. W., and M. Shirzaei (2021). More than 40 yr of potentially induced seismicity close to the San Andreas fault in San Ardo, Central California, *Seismol. Res. Lett.* **92,** 187–198.

González, G., E. Fujita, B. Shibazaki, T. Hayashida, G. Chiodini, F. Lucchi, I. Yokoyama, K. Nemeth, R. Mora-Amador, A. Moya, *et al.* (2021). Increment in the volcanic unrest and number of eruptions after the 2012 large earthquakes sequence in Central America, *Sci. Rep.* **11,** 22,417.

Granieri, D., G. Salerno, M. Liuzzo, A. L. Spina, G. Giuffrida, T. Caltabiano, G. Giudice, E. Gutierrez, F. Montalvo, M. R. Burton, *et al.* (2015). Emission of gas and atmospheric dispersion of so2 during the December 2013 eruption at San Miguel volcano (El Salvador, Central America), *Geophys. Res. Lett.* **42,** 5847–5854.

Harlow, D. H., R. A. White, R. Michael, and S. G. Alvarez (1993). The San Salvador earthquake of 10 October 1986 and its historical context, *Bull. Seismol. Soc. Am.* **83,** 1143–1154.

Hernández, P. A., N. M. Pérez, J. C. Varekamp, B. Henriquez, A. Hernández, J. Barrancos, E. Padrón, D. Calvo, and G. Melián (2007). Crater lake temperature changes of the 2005 eruption of Santa Ana volcano, El Salvador, Central America, *Pure Appl. Geophys.* **164,** 2507–2522.

Herrera, R., F. Montalvo, A. Herrera, and S. Tecla (2010). El Salvador country update, *Proc. of the World Geothermal Congress*, 1–6.

Kissling, E., W. L. Ellsworth, D. Eberhart-Phillips, and U. Kradolfer (1994). Initial reference models in local earthquake tomography, *J. Geophys. Res.* **99,** 19,635–19,646.

Krischer, L., T. Megies, R. Barsch, M. Beyreuther, T. Lecocq, C. Caudron, and J. Wassermann (2015). Obspy: a bridge for seismology into the scientific python ecosystem, *Comput. Sci. Discov.* **8,** 014003.

Kwiatek, G., F. Bulut, M. Bohnhoff, and G. Dresen (2014). High-resolution analysis of seismicity induced at Berlín geothermal field, El Salvador, *Geothermics* **52,** 98–111.

Laiolo, M., D. Coppola, F. Barahona, J. E. Benítez, C. Cigolini, D. Escobar, R. Funes, E. Gutierrez, B. Henriquez, A. Hernandez, *et al.* (2017). Evidences of volcanic unrest on high-temperature fumaroles by satellite thermal monitoring: The case of Santa Ana volcano, El Salvador, *J. Volcanol. Geotherm. Res.* **340,** 170–179.

Legrand, D., G. Marroquín, C. DeMets, L. Mixco, A. García, M. Villalobos, D. Ferrés, E. Gutiérrez, D. Escobar, R. Torres, *et al.* (2020). Active deformation in the San Salvador extensional stepover, El Salvador from an analysis of the April-May 2017 earthquake sequence and GPS data, *J. South Am. Earth Sci.* **104,** 102,854.

Lomax, A., A. Michelini, and A. Curtis (2009). Earthquake location, direct, global-search methods, in *Encyclopedia of Complexity and System Science*, R. A. Meyers, Springer, New York, NY, 2449–2473.

Manconi, A., V. Coviello, M. Galletti, and R. Seifert (2018). Short communication: Monitoring rockfalls with the raspberry shake, *Earth Surf. Dynam.* **6,** 1219–1227.

Martínez-Díaz, J. J., J. A. Álvarez Gómez, B. Benito, and D. Hernández (2004). Triggering of destructive earthquakes in El Salvador, *Geology* **32,** 65.

McNutt, S. R. (2005). Volcanic seismology, *Annu. Rev. Earth Planet. Sci.* **33,** 461–491.

Olmos, R., J. Barrancos, C. R. Ivera, F. Barahona, D. L. López, B. Henriquez, A. Hernández, E. Benitez, P. A. Hernández, N. M. Pérez, *et al.* (2007). Anomalous emissions of so2 during the recent eruption of Santa Ana volcano, El Salvador, Central America, *Pure Appl. Geophys.* **164,** 2489–2506.

Parsons, T. (2002). Global omori law decay of triggered earthquakes: Large aftershocks outside the classical aftershock zone, *J. Geophys. Res.* **107,** ESE 9-1–ESE 9-20.

Pullinger, C. (1998). Evolution of the Santa Ana volcanic complex, El Salvador, *Master of Science in Geology*, Michigan Technological University, 1–148.

Rose, W. I., and R. E. Stoiber (1969). The 1966 eruption of Izalco volcano, El Salvador, *J. Geophys. Res.* **74,** 3119–3130.

Scolamacchia, T., C. Pullinger, L. Caballero, F. Montalvo, L. E. B. Orosco, and G. G. Hernández (2010). The 2005 eruption of ilamatepec (Santa Ana) volcano, El Salvador, *J. Volcanol. Geotherm. Res.* **189,** 291–318

SeisComP (2008). The SeisComp seismological software package, *GFZ Data Services*, doi: 10.5880/GFZ.2.4.2020.003.

Shi, Y., and B. A. Bolt (1982). The standard error of the magnitude-frequency b-value, *Bull. Seismol. Soc. Am.* **72,** 1677–1687.

Siebert, L., P. Kimberly, and C. R. Pullinger (2004). The voluminous Acajutla debris avalanche 1664 from Santa Ana volcano, western El Salvador, and comparison with other Central American edifice-failure events, Geological Society of America Special Paper, W. I. Rose, J. J. Bommer, D. L. López, M. J. Carr, and J. J. Major (Editors), Vol. 375, Natural Hazards, El Salvador, 5–23.

Trugman, D. T., and P. M. Shearer (2017). Growclust: A hierarchical clustering algorithm for relative earthquake relocation, with application to the Spanish springs and Sheldon, Nevada, earthquake sequences, *Seismol. Res. Lett.* **88,** 379–391.

Walter, J. I., P. Ogwari, A. Thiel, F. Ferrer, I. Woelfel, J. C. Chang, A. P. Darold, and A. A. Holland (2019). The Oklahoma geological survey statewide seismic network, *Seismol. Res. Lett.* **91,** no. 2A, 611–621.

Ye, L., T. Lay, and H. Kanamori (2013). Large earthquake rupture process variations on the middle America megathrust, *Earth Planet. Sci. Lett.* **381,** 147–155.

Zaliapin, I., and Y. Ben-Zion (2013a). Earthquake clusters in southern California I: Identification and stability, *J. Geophys. Res.* **118,** 2847–2864.

Zaliapin, I., and Y. Ben-Zion (2013b). Earthquake clusters in southern California II: Classification and relation to physical properties of the crust, *J. Geophys. Res.* **118,** 2865–2877.

Zaliapin, I., and Y. Ben-Zion (2016). Discriminating characteristics of tectonic and human-induced seismicity, *Bull. Seismol. Soc. Am.* **106,** 1–14.

Manuscript received 3 September 2024
Published online 12 March 2025